Iterative Physical Optics for Radar Scattering Predictions

Robert J. Burkholder [1], Çağatay Tokgöz [2], C. J. Reddy [2], and William O. Coburn [3]

[1] Department of Electrical and Computer Engineering
The Ohio State University, Columbus, OH 43212, USA
burkholder.1@osu.edu

[2] Applied EM, Inc., Hampton, VA 23666, USA
cagatay@appliedem.com, cjreddy@appliedem.com

[3] U. S. Army Research Laboratory, Aberdeen Proving Ground, MD, USA
wcoburn@arl.army.mil

Abstract─ The iterative physical optics (IPO) method is applied to compute the radar cross section of electrically large and realistically complex targets. The method is based on iterative refinement of the first-order physical optics currents to include multiple interactions up to a specified order. Unlike other high-frequency asymptotic methods, no ray tracing is required, and spurious diffraction effects from non-physical shadow boundaries are avoided. Numerical results are presented to demonstrate convergence, accuracy, efficiency and robustness.

Index Terms─ Physical optics, radar cross section, iterative methods, integral equations, high-frequency methods.

I. INTRODUCTION

The prediction of the radar cross section (RCS) of realistic targets remains a computational challenge due to the large size and complexity of aircraft, ships and ground vehicles. It is of considerable interest to develop efficient, robust and accurate computational electromagnetic (EM) methods to address this problem. In this article, the iterative physical optics (IPO) technique, previously developed for jet inlet scattering, is adapted to more general computer-aided design (CAD) geometries [1-3].

In the past, both numerical and ray tracing methods have been applied to RCS prediction. Numerical methods such as the method of moments (MoM) and the finite element-boundary integral (FE-BI) method are very accurate and reasonably robust for analyzing faceted CAD geometries [4,5]. However, the computational cost becomes extremely high for the electrically large problems that are typically of interest for radar scattering. For example, a fighter-size aircraft is on the order of a thousand wavelengths in length at X-band frequencies. A surface mesh of such a target requires upwards of 10 million unknowns. This size of problem has been solved by using the multi-level fast multi-pole algorithm, but requires massive parallel computing resources and a highly sophisticated software implementation [6]. Similarly, a volume mesh for finite element based methods typically requires hundreds of millions of unknowns. While domain decomposition methods for the FEM have come a long way in providing sparser matrices [7] and some very large problems have been solved [8], such solutions are still far from routine for most RCS engineers.

Physical optics (PO) based methods have provided engineers with a useful alternative to numerical methods for generating fast results, but at the cost of decreased accuracy. First-order PO includes the direct reflection and diffraction by the target from the PO approximation of the induced surface currents, as illustrated in Fig. 1(a). Only the optically lit part of the geometry has non-zero currents. It is noticed from Fig. 1(a) that this introduces abrupt shadow boundaries that, when integrated, give rise to false edge diffraction effects. It is also noticed that the strong double-bounce from the dihedral corner reflector is not included in the first-order PO.
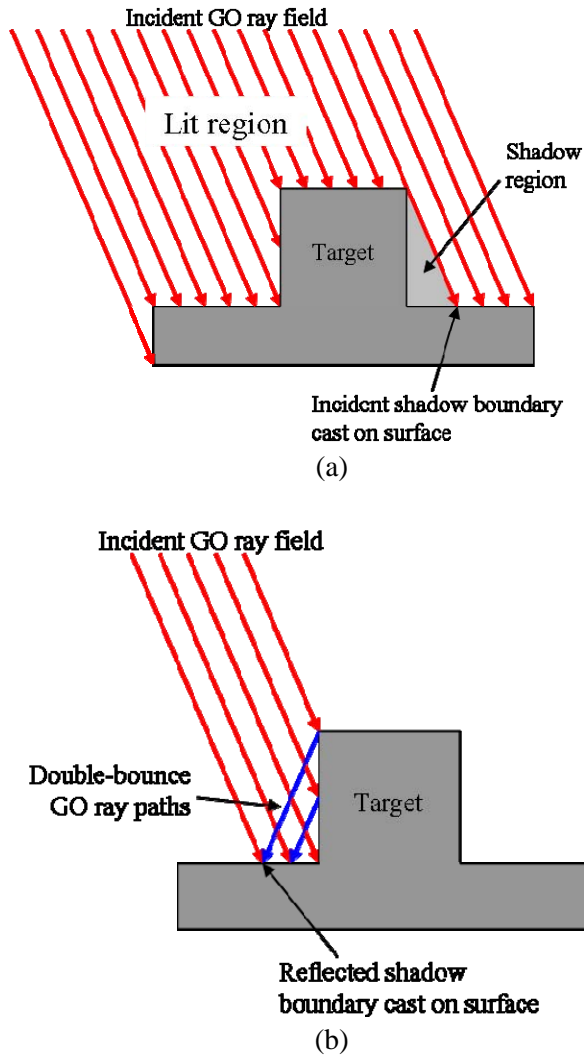
Fig. 1. GO/PO illumination of a multi-bounce RCS target: (a) First-order PO ray paths due to plane wave illumination on an RCS target. (b) Double-bounce ray paths associated with an RCS target.

To add multi-bounce effects, geometrical optics (GO) has been combined with PO in the shooting and bouncing ray (SBR) method [9], or GO/PO [10-12]. It is interesting to note that the SBR method was also originally developed for cavity scattering, similar to IPO. The incident field is represented as a set of GO rays which are launched at the target and traced through multiple reflections. At each bounce point, the ray footprint is integrated via PO [13]. This is the method used in the popular Xpatch suite of codes [14]. Figure 1(b) illustrates the strong double-bounce mechanism associated with the target which would be included by using SBR. However, it is noticed that the first GO bounce gives rise to another

abrupt shadow boundary on the second surface which also gives rise to a false diffraction. In reality, these shadow boundaries are smoothed out by the continuous nature of the EM field as explained by the uniform geometrical theory of diffraction (UTD) [15]. The false diffractions in the SBR method can be misinterpreted as real scattering centers by target recognition algorithms [16].

IPO provides a way to include multi-bounce while not introducing false shadow boundaries. It does not use ray tracing and can be applied to general faceted CAD geometries. It is not quite as efficient as ray based methods since it requires integration, but it is far more efficient than numerical methods because the mesh density is coarser, only a certain percentage of the total surface area will be excited and simultaneous solution of matrix equations is not required. The basic approach is to start with first-order PO currents ignoring shadowing effects, and iteratively integrating the currents by using a simple facet visibility check. The iteration is halted after a prescribed number of bounces is reached or the IPO currents converge. The algorithm is described in Section II and implementation techniques are discussed in Section III. The convergence and accuracy of the method are demonstrated in the numerical results of Section IV.

II. THE IPO ALGORITHM

As its name implies, IPO iteratively refines the PO currents to account for multiple reflections and diffractions within the high-frequency asymptotic assumptions of PO. It is assumed that the target is a perfect electric conductor (PEC), but the formulation can be easily modified for impenetrable material surfaces [3,17]. In the following, an $e^{j\omega t}$ harmonic time convention is assumed and suppressed where ω is the radian frequency of the incident EM wave. The ambient medium is free space with EM wave number, $k = \omega / c$, where c is the speed of light in free space.
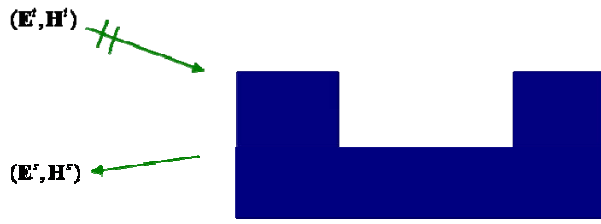
Consider the plane wave scattering problem shown in Fig. 2(a). The PO approximation is based on the magnetic field integral equation [4]. The equivalent current at a point **r** on the surface S of the target is found by solving the following MFIE,

$$\mathbf{J}(\mathbf{r}) = 2\hat{\mathbf{n}} \times \mathbf{H}^i(\mathbf{r}) + 2\hat{\mathbf{n}} \times \mathbf{H}(\mathbf{J}), \qquad (1)$$

where $\mathbf{H}^i(\mathbf{r})$ is the incident magnetic field and $\hat{\mathbf{n}}$ is the outward-pointing unit normal vector. $\mathbf{H}(\mathbf{J})$ is the principal value magnetic field radiation integral given by,

$$\mathbf{H}(\mathbf{J}) = P\int_S \mathbf{J}(\mathbf{r}') \times \hat{\mathbf{R}}' \frac{e^{-jkR'}}{4\pi R'}\left(jk + \frac{1}{R'} \right) dS', \quad (2)$$

where $\mathbf{R}' = \mathbf{r} - \mathbf{r}'$, $R' = |\mathbf{R}'|$ and $\hat{\mathbf{R}}' = \mathbf{R}'/R'$. The primed quantities represent variables of integration. Figure 2(b) shows the equivalent current representation of the scattering problem. The currents radiate the scattered fields $(\mathbf{E}^s, \mathbf{H}^s)$ in free space.

(a) Plane wave scattering problem.
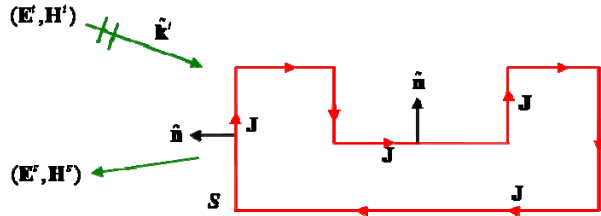
(b) Equivalent currents radiating in free space.

Fig. 2. Equivalent current representation of the plane wave scattering from a simple concave geometry.

The first-order PO approximation used here is,

$$\mathbf{J}^{(0)}(\mathbf{r}) = \begin{cases} 2\hat{\mathbf{n}} \times \mathbf{H}^i(\mathbf{r}) : \hat{\mathbf{n}} \cdot \hat{\mathbf{k}}^i < 0 \\ 0 \qquad : \hat{\mathbf{n}} \cdot \hat{\mathbf{k}}^i \ge 0 \end{cases}, \qquad (3)$$

where $\hat{\mathbf{k}}^i$ is the unit propagation vector of the incident plane wave. It is noted that the first-order currents are non-zero only where the unit normal vector is facing towards the incident plane wave,

regardless of any intervening geometry. In the classical PO method, shadowing by other portions of the surface must be taken into account as shown in Figure 1(a). In IPO, only the facing direction of each facet is checked relative to the direction of incidence. This obviously puts first-order currents inside the incident shadow region where they do not belong, as shown in Figure 3(a) on surface, S_2. However, this is only the initial set of currents for the IPO algorithm.
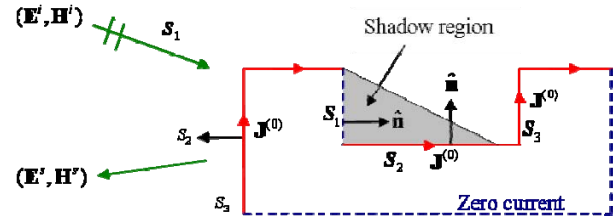
(a) Initial IPO currents.
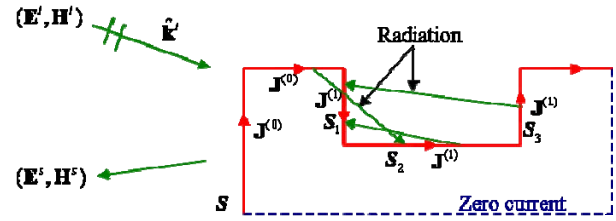
(b) IPO currents after the first iteration.

Fig. 3. IPO currents on a concave structure.

The IPO algorithm solves the modified PO equivalent of the MFIE of (1) as,

$$\mathbf{J}(\mathbf{r}) = \mathbf{J}^{(0)}(\mathbf{r}) + 2\hat{\mathbf{n}} \times \mathbf{H}_{IPO}(\mathbf{J}), \qquad (4)$$

where the IPO definition of the magnetic field radiation integral is given by,

$$\mathbf{H}_{IPO}(\mathbf{J}) = P\int_{\hat{\mathbf{n}} \cdot \hat{\mathbf{R}}' < 0} \mathbf{J}(\mathbf{r}') \times \hat{\mathbf{R}}' \frac{e^{-jkR'}}{4\pi R'}\left(jk + \frac{1}{R'} \right) dS'. $$
$$(5)$$

It is noticed that this is the same as (2), but the integration is only over the portion of the surface where $\hat{\mathbf{n}} \cdot \hat{\mathbf{R}}' < 0$, which is the *IPO shadowing rule*. This rule is applied only to test points on the surface. By definition the equivalent currents

radiate in free space regardless of which way they are facing. The IPO shadowing rule is one property that makes IPO much more efficient than the conventional MoM, because only a small fraction of the whole surface radiates to a given test point on the surface.

Classical Jacobi iteration may be used to solve (4) [18]. At the qth iteration the currents are given by

$$\mathbf{J}^{(q)}(\mathbf{r}) = \mathbf{J}^{(0)}(\mathbf{r}) + 2\hat{\mathbf{n}} \times \mathbf{H}_{IPO}(\mathbf{J}^{(q-1)}). \qquad (6)$$

Accordingly, the currents for the first iteration shown in Figure 3(b) are given by,

$$\mathbf{J}^{(1)}(\mathbf{r}) = \mathbf{J}^{(0)}(\mathbf{r}) + 2\hat{\mathbf{n}} \times \mathbf{H}_{IPO}(\mathbf{J}^{(0)}). \qquad (7)$$

As the radiation arrows show, the first-order currents on the lit outer surface of the target radiate to the concave part on S_1, S_2 and S_3. This radiation tends to cancel the incident field on S_2, thus filling in the shadow region with a continuous field. The original currents on S_2 and S_3 also radiate into the concave region. However, these currents do not radiate to the outer surface because of the IPO shadowing rule.

As the iteration is continued, the currents in the concave region will eventually converge. The iteration may be halted after a prescribed number of interactions are included, or a convergence criterion is reached. A useful error convergence definition is,

$$\frac{\left\| \mathbf{J}^{(q)} - \mathbf{J}^{(q-1)} \right\|}{\left\| \mathbf{J}^{(0)} \right\|} < \varepsilon , \qquad (8)$$

assuming $\left\| \mathbf{J}^{(0)} \right\| > 0$. Alternatively, the convergence of the scattered field may be monitored.

Each iteration of the IPO algorithm essentially adds another multi-bounce term. Thus, IPO intrinsically includes an arbitrary number of interactions, and shadow regions are filled in without abrupt shadow boundaries. If the algorithm diverges for some cases, a relaxed Jacobi version of (7) may be used as,

$$\mathbf{J}^{(q)}(\mathbf{r}) = \frac{1}{2}\mathbf{J}^{(0)}(\mathbf{r}) + \frac{1}{2}\mathbf{J}^{(q-1)} + \hat{\mathbf{n}} \times \mathbf{H}_{IPO}(\mathbf{J}^{(q-1)}). \qquad (9)$$

In fact, there are many forms of classical iterative algorithms that have been found to work well with IPO, such as Gauss-Seidel and successive over-relaxation [18]. A forward-backward version of IPO (FBIPO) was presented for inlet cavity scattering in [3]. That version was found to have the best convergence for geometries with a very high degree of multi-bounce. FBIPO is technically the same as the method of symmetric successive over-relaxation. Krylov subspace methods based on minimizing the residual error of the matrix equation have also been investigated [2]. However, these methods have not been successful with IPO because the IPO operator of (5) is not analytic due to the IPO shadowing rule. Also, the simple physical interpretation of IPO is lost on such methods.

III. IMPLEMENTATION

PO currents by nature do not have the strong singularities that may be present in MoM solutions, and hence, the radiation integral of (5) may be evaluated numerically by point sampling. This makes the IPO method easy to implement on faceted CAD geometries if the surface mesh is made on the order of the required numerical sampling density. Then, only one point per facet is needed. Because of the smoothness of the PO currents, it has been found that a sampling density of 9 to 16 points per square wavelength yields very good accuracy [1]. This is in contrast to MoM and FEM discretization which typically requires a minimum sampling density of 64 to 100 points per square wavelength.

With point sampling of the currents and point-wise numerical integration, it is easy to evaluate (6) as

$$\mathbf{J}^{(q)}(\mathbf{r}_m) = \mathbf{J}^{(0)}(\mathbf{r}_m) + \sum_{n=1}^{N} 2A_n \hat{n} \times \left[\mathbf{J}^{(q-1)}(\mathbf{r}_n) \times \hat{\mathbf{R}}_{mn} \right]$$
$$\cdot \frac{e^{-jkR_{mn}}}{4\pi R_{mn}} \left(jk + \frac{1}{R_{mn}} \right) \Bigg|_{\substack{n \neq m \\ \hat{\mathbf{n}} \cdot \hat{\mathbf{R}}_{mn} < 0}} , \qquad (10)$$

where A_n is the area of the nth facet, $\mathbf{r}_n$ is the vector to the center of the nth facet and $\mathbf{R}_{mn} = \mathbf{r}_m - \mathbf{r}_n$. It is possible to rewrite (10) in matrix format in order to store a system matrix. However, since there may be a very large number of facets and the

expression in the summation does not require numerical integration of a basis function, it has been found to be more practical to recompute the terms on the fly for each iteration. The extra cost of this operation is ameliorated by performing the iterative solution for multiple excitations simultaneously. Then, only the currents themselves need to be stored. Therefore, the memory requirement is O(N).

Fast Far-Field Approximation

The computational cost of the operation of (10) is still O(N^2), even though only a fraction of the facets contribute to any given test point. To reduce the cost to O($N^{3/2}$), the fast far-field approximation (FaFFA) [19] may be applied as described in [2]. Similar to the fast multi-pole method [20], the geometry is broken up into small groups of facets. Contributions from receiving groups that are in the far-field of the transmitting group are computed by using the far-field approximation which naturally factorizes the Green's function in the radiation kernel. The interactions between near-field groups are computed in the usual fashion. FaFFA has been found to reduce the computation time by an order of magnitude in practical applications.

Model Based Parameter Estimation

The efficiency of IPO for RCS pattern computations has been further improved by using it in conjunction with adaptive Model Based Parameter Estimation (MBPE) for fast angle or frequency sweeps [21]. MBPE has been used to accelerate the RCS computation when only an angle or frequency is swept. When MBPE is used, the coefficients of the surface currents are approximated by a ratio of Mth and N^{th} order polynomials as

$$c(\alpha) \approx \frac{\sum_{m=0}^{M} a_m \alpha^m}{1 + \sum_{n=1}^{N} b_n \alpha^n}, \qquad (11)$$

where α is the angle or frequency that is swept, $c(\alpha)$ is a surface current coefficient, and a_m and b_n are unknowns to be determined. Since there are $L = M + N + 1$ unknowns, values of each surface current coefficient are evaluated at L sample points uniformly distributed within the range of α to solve for these unknowns. After the unknowns are determined, RCS values computed by using (11) and those obtained without MBPE are compared at midpoints between sample points to check the accuracy of the MBPE implementation. If the MBPE implementation is not sufficiently accurate in magnitude and phase at all the midpoints, the range of α is divided into two equal subintervals, and MBPE is applied in each subinterval again. This procedure of dividing each interval into two equal subintervals, applying MBPE in each subinterval and checking the accuracy at midpoints of all MBPE subintervals is adaptively repeated until the desired accuracy is achieved at all the midpoints. The adaptive MBPE algorithm is illustrated in Fig. 4.
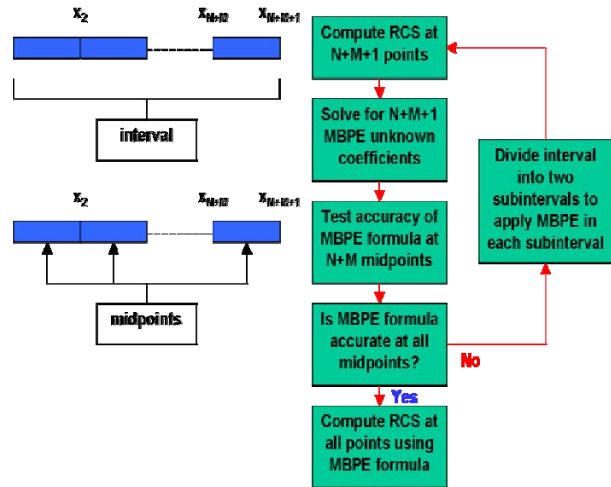

Fig. 4. Adaptive MBPE algorithm.

An RCS prediction code named rcsASET was developed based on IPO. The rcsASET code was parallelized with Message Passing Interface (MPI) and ported to SGI, IBM and Linux platforms at the Major Shared Resource Center (MSRC) of the U.S. Army Research Laboratory (ARL). The code was validated, and its efficiency and accuracy in RCS computation were demonstrated by computing the RCS of several benchmark targets for various frequencies and scattering angles, and comparing the results with those generated by using other software or measured data. In summary, the IPO method gets its efficiency from the following factors:

1. Memory requirement is O(N),
2. IPO shadowing rule greatly reduces the number of facet-to-facet interactions,
3. Numerical sampling density is only 9 to 16 points per square wavelength,
4. Number of iterations is related to the number of significant multi-bounce terms,
5. Fast far-field approximation accelerates summations,
6. Model based parameter estimation minimizes the number of RCS pattern points,
7. Parallelization helps reduce the computation time.

These properties allow the IPO method to routinely handle RCS problems involving electrically large and realistically complex structures.

IV. NUMERICAL RESULTS

The results of this section demonstrate the efficiency, accuracy and convergence of the IPO algorithm for several practical examples. Following that, the MBPE technique is applied to reduce the number of RCS data points necessary to generate a continuous pattern.

Trihedrals

The first case demonstrates convergence in terms of the number of iterations. Figure 5 shows the mono-static RCS vs. azimuth patterns of a 1 m square trihedral for an elevation angle of 45° at a frequency of 1 GHz comparing IPO with a method of moments (MoM) reference solution. The incident polarization is vertical. The levels are in very good agreement, even in angular regions where the concave side of the trihedral is partially shadowed, such as in the range 90° and 180°. The agreement in cross-polarization is also very good.

Figure 6 shows the RCS patterns for the same trihedral for different iterations. The solid curve is the converged IPO result which took 5 iterations. The dashed curve is for zero iterations, which is simply the first-order PO result. First-order PO only predicts the direct scattering and not the multi-bounce, so it agrees well with the converged solution only in angular regions where the multi-bounce is not significant. Note that first-order PO predicts a zero cross-polarization component, so it is not included in the cross-polarization plot. The dot-dash curves are for 1 iteration, which includes

the second-order terms corresponding to double-reflection, double-diffraction, reflection-diffraction and diffraction-reflection (in addition to the first-order terms). The 1 iteration curves agree well with the converged solution where the dihedral reflection is dominant, such as around 0° and 90° azimuth. Also note the region between 90° and 180° where the concave side of the trihedral is partially shadowed. IPO with 1 iteration predicts this well, whereas the first-order PO solution does not. The dotted curves are for 2 iterations, which includes the third-order terms (in addition to the first and second-order terms). The triple-bounce off the trihedral is dominant in the angular 0° to 90°, which is predicted very well with 2 iterations of IPO. These results demonstrate how each iteration of IPO adds the next higher-order interaction terms.
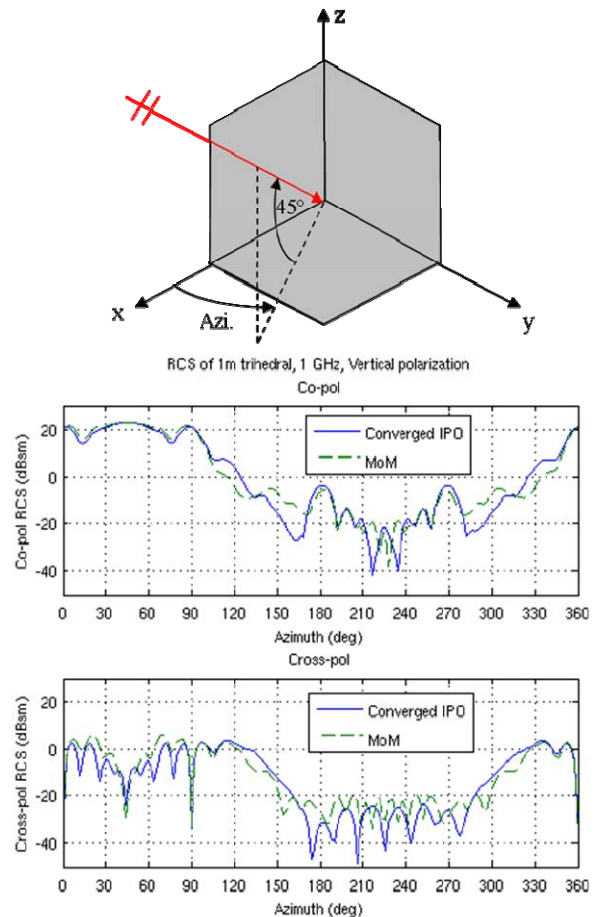

Fig. 5. Mono-static RCS patterns of a 1 m square PEC trihedral computed with IPO and MoM. Frequency is 1 GHz, elevation is 45° and the incident polarization is vertical.

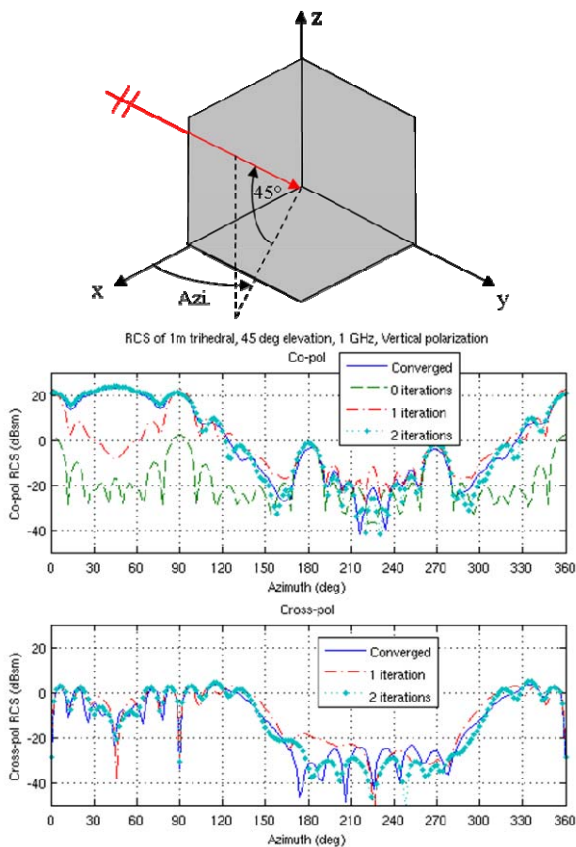RCS of 1m trihedral, 45 deg elevation, 1 GHz, Vertical polarization

Fig. 6. Convergence of RCS patterns of a 1 m square PEC trihedral computed with IPO. Frequency is 1 GHz, 45° elevation, and the incident polarization is vertical. Cross-polarization for 0 iterations is not plotted because it is identically zero.

First, the mono-static RCS of a tilted trihedral, which is 142.24 x 60.96 x 20.32 cm in size as shown in Fig. 7, was computed by using IPO at 3 and 9 GHz for 0-90° azimuth, 10° elevation, and co-polarized fields. CAD models for this target consist of 1,169 and 10,078 triangular facets at 3 and 9 GHz, respectively, corresponding to about 10 facets per square wavelength. There is a good agreement between IPO results and the results obtained by using MLFMM available from electromagnetic simulation software, FEKO, as shown in Fig. 8 at 3 GHz. The mesh for the MLFMM results required 14,357 triangular facets corresponding to about 123 facets per square wavelength at 3 GHz, which is typical of purely numerical methods. The IPO results also compare well with measured data as shown in Fig. 9 at 9 GHz. It is noted that the measured data is averaged
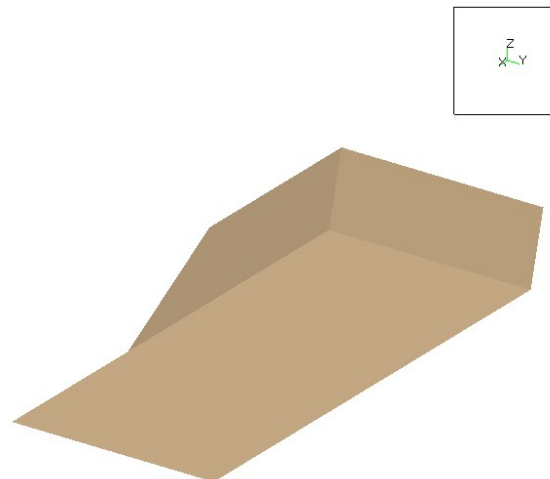
Fig. 7. CAD model for the tilted trihedral.
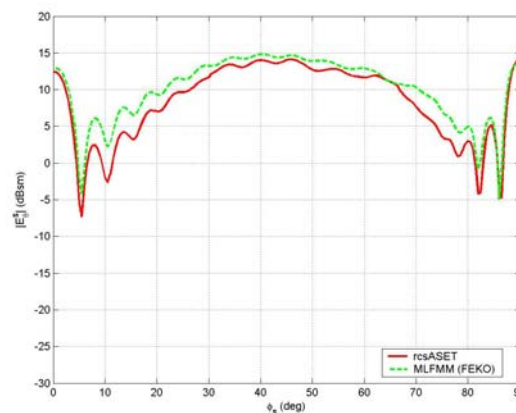
(a) Vertical polarization.
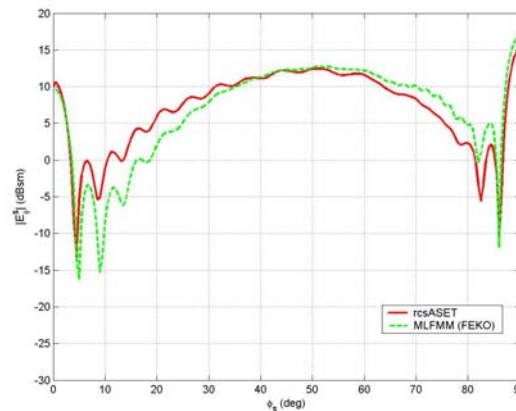
(b) Horizontal polarization.

Fig. 8. IPO results for co-polarized mono-static RCS of the tilted trihedral compared to the MLFMM results obtained by using FEKO for 0-90° azimuth and 10° elevation at 3 GHz.
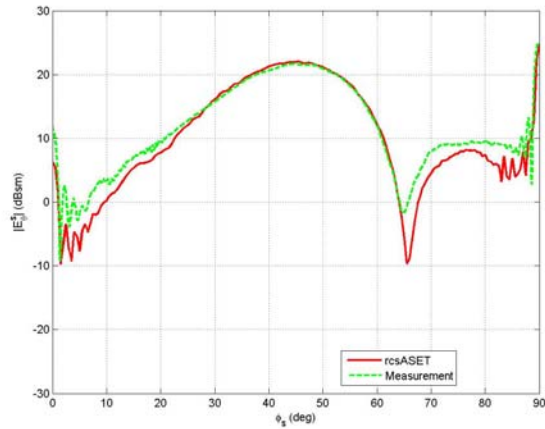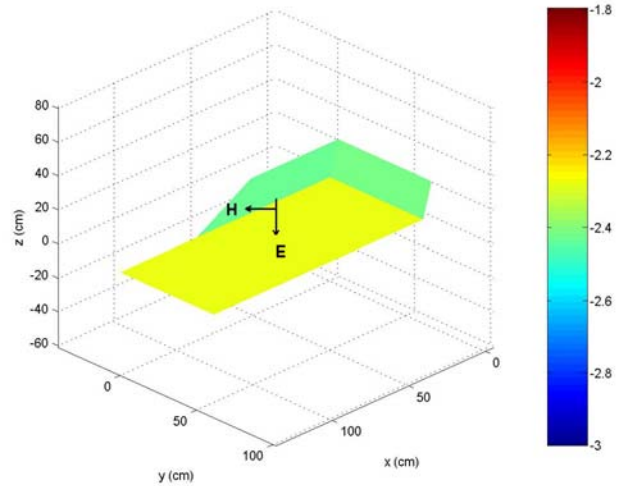
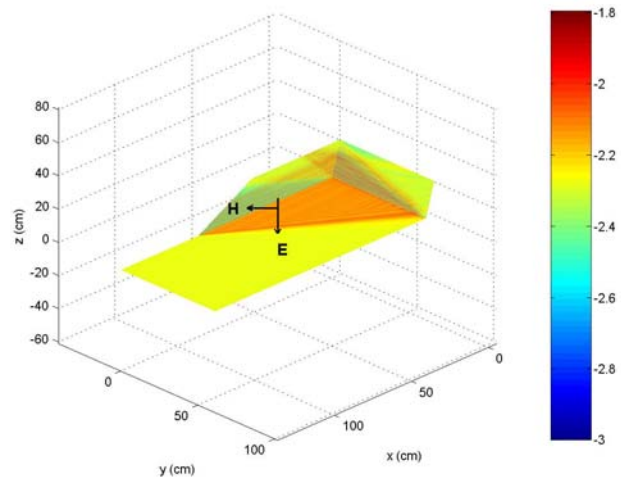(a) Vertical polarization.
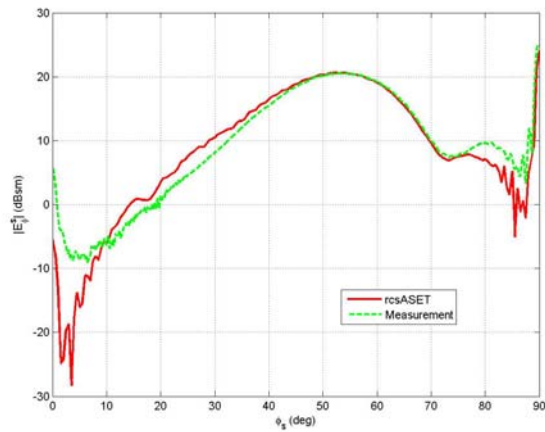
(b) Horizontal polarization.

Fig. 9. IPO results for co-polarized mono-static RCS of the tilted trihedral compared to measured data for 0-90° azimuth and 10° elevation at 9 GHz. Measured data is averaged over a 1 GHz bandwidth.

over a 1 GHz bandwidth [22]. Since IPO takes multi-bounce into consideration, it can capture the null in Fig. 9(a) which cannot be captured properly by using only PO. First-order PO and converged IPO current distributions at 94 GHz for 45° azimuth and 10° elevation are shown in Fig. 10. IPO currents exhibit a standing wave behavior due to multi-bounce as expected, whereas PO currents do not show such behavior.

A smooth corner trihedral shown in Fig. 11 was considered next. Unlike the tilted trihedral, plates forming the smooth corner trihedral are perpendicular to each other and have finite thicknesses. Mono-static RCS of this target, which is 62.00 x 62.00 x 31.40 cm in size, was computed

(a) First-order PO currents.

(b) Converged IPO currents.

Fig. 10. Surface current distributions over the tilted trihedral for 45° azimuth, 10° elevation and vertical polarization at 94 GHz.

by using IPO at 9 GHz for co-polarized fields. The CAD model for the target consists of 7,064 triangular facets at this frequency, corresponding to about 10 facets per square wavelength. IPO results compare well with measured data as shown in Figure 12 for 0-90° azimuth and 10° elevation. It is noted that the measured data was obtained in the near-field of the trihedral, which explains the shift in the peak near 90° [23]. Moreover, first-order PO and converged IPO current distributions at 94 GHz for 45° azimuth and 10° elevation are shown in Fig. 13, which respectively behave similar to the PO and IPO currents over the tilted trihedral shown in Fig. 9.
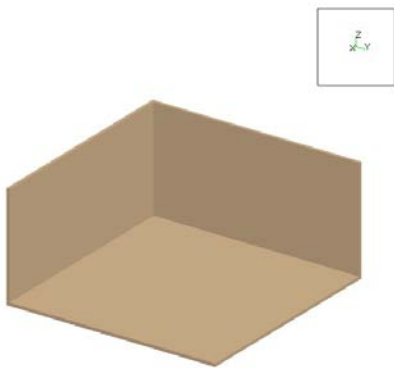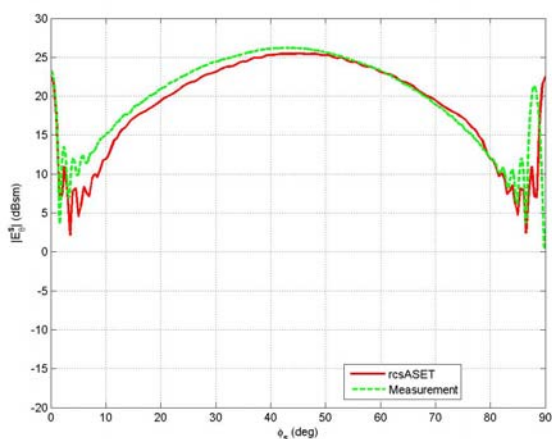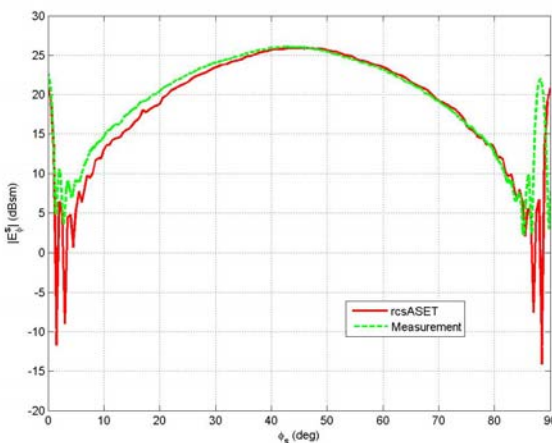
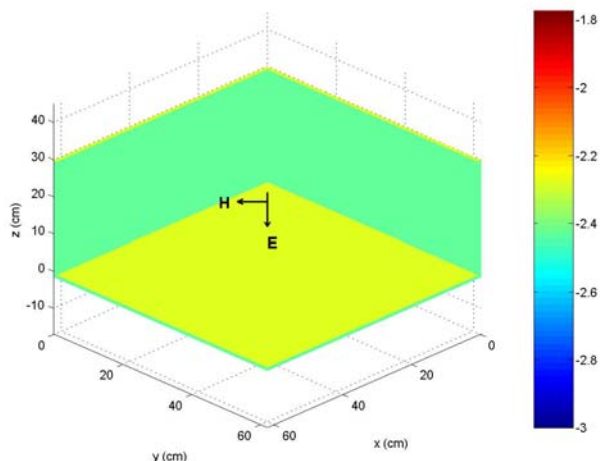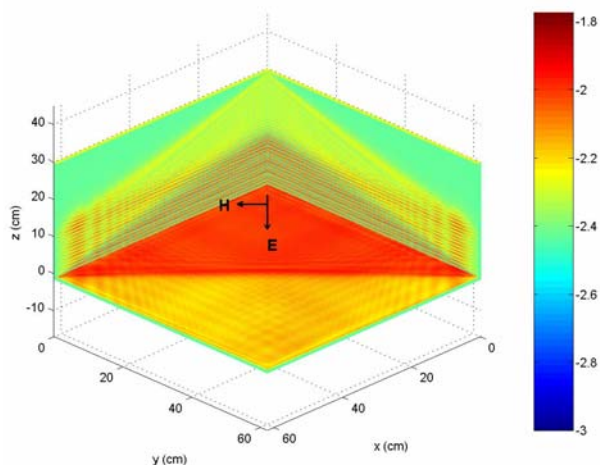Fig. 11. CAD model for the smooth corner trihedral.

(a) First-order PO currents.

(a) Vertical polarization.

(b) Converged IPO currents.

Fig. 13. Surface current distributions over the smooth corner trihedral for 45° azimuth, 10°elevation and vertical polarization at 94 GHz.

SLICY

The mono-static RCS of another target shown in Fig. 14 was also computed. This target is historically known as DICY since it consists of canonical shapes such as dihedrals and cylinders. It was later used by Sandia National Laboratories where it was renamed SLICY. The mono-static RCS of this target, which is 244.49 x 275.05 x 167.96 cm in size, was computed by using IPO at 9 GHz for co-polarized fields. The CAD model for the target consists of 322,468 triangular facets at this frequency, corresponding to more than 12 facets per square wavelength. IPO results are shown in comparison with the results obtained by using electromagnetic simulation software, XPatch, in Fig. 15 for 0-360° azimuth while

(b) Horizontal polarization.

Fig. 12. IPO results for co-polarized mono-static RCS of the smooth corner trihedral compared to measured data for 0-90° azimuth and 10° elevation at 9 GHz. Measured data was obtained in the near-field of the trihedral.

elevation is 10° and 30° for vertical and horizontal polarizations, respectively. It is noted that the XPatch results are averaged over a 1 GHz bandwidth. The IPO results were found to be close to the measured data (not shown) whereas Xpatch underestimates the RCS by 2-3 dB in the 90-270° azimuth range since it can not account for the third bounce properly. First-order PO and converged IPO current distributions at 9 GHz for 225° azimuth and 10° elevation are also shown in Fig. 16.
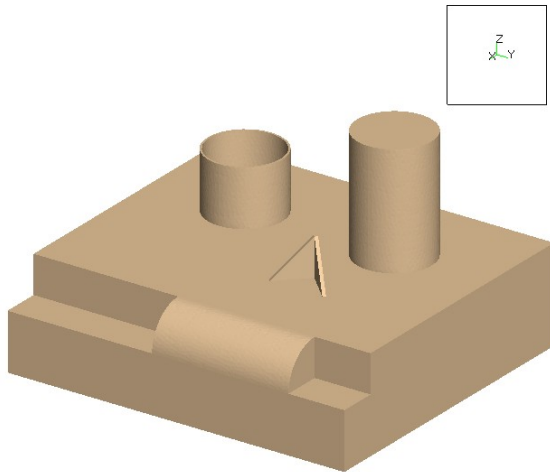
Fig. 14. CAD model for SLICY.

ZSU-23-4 Anti-Aircraft Tank

The mono-static RCS of an anti-aircraft tank, ZSU-23-4, shown in Fig. 17 was also studied. The mono-static RCS of this target, which is 598.5 x 308.7 x 364.3 cm in size, was computed by using IPO at 2 and 9 GHz for 0-360° azimuth, 30° elevation and co-polarized fields. The CAD model for IPO consists of 118,712 triangular facets at 2 GHz, corresponding to about 10 facets per square wavelength. The IPO results compare well with the results obtained by using electromagnetic simulation software, Maxwell Solver Physical Optics (MSPO), as shown in Fig. 18 at 2 GHz. The IPO results are also consistent with measured data as shown in Fig. 19 at 9 GHz. It should be noted that the IPO results are angle averaged whereas the measured data are frequency averaged over a 2 GHz bandwidth. Also, the measurements were performed with the target on an absorber-covered in-ground turntable [24], whereas the IPO results for this case are in free space. This explains the discrepancies in the details of the patterns,

whereas the envelope levels are in good agreement. A coarse CAD model with 1,027,796 triangular facets, corresponding to less than 10 facets per square wavelength, has been used at 9 GHz to reduce computation time. It has been observed that good accuracy can be achieved with IPO if a minimum of 4-9 facets per square wavelength are used. First-order PO and converged IPO current distributions at 9 GHz for 0° azimuth and 15° elevation are also shown in Figure 20.
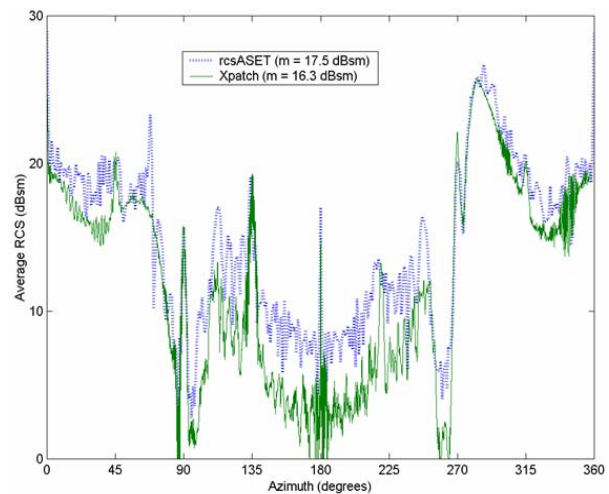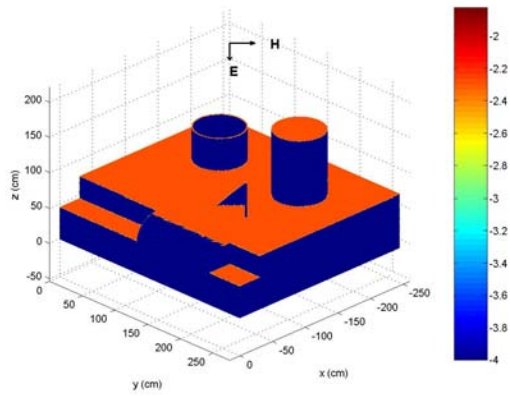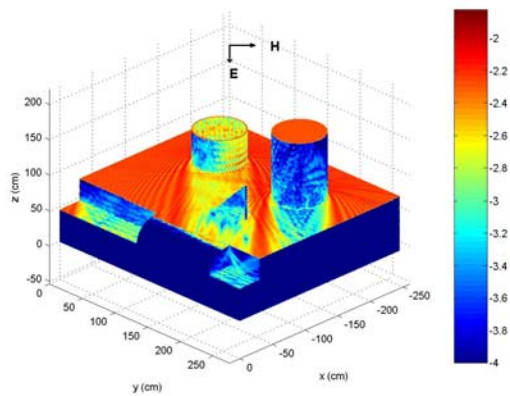

(a) Vertical polarization for 10° elevation.
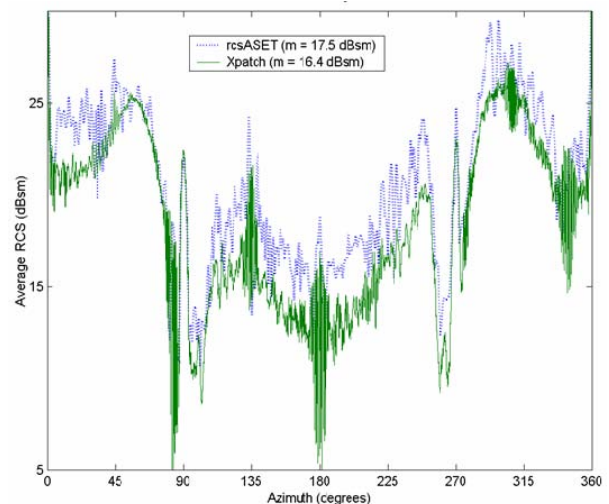
(b) Horizontal polarization for 30° elevation.

Fig. 15. IPO results for co-polarized mono-static RCS of SLICY compared to the results obtained by using XPatch for 0-360° azimuth at 9 GHz. Xpatch results are frequency averaged over a 1 GHz bandwidth.
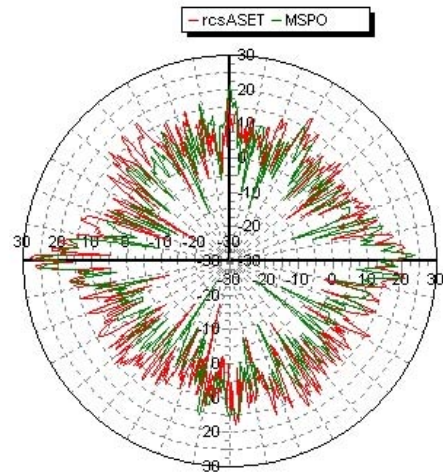
(a) First-order PO currents.

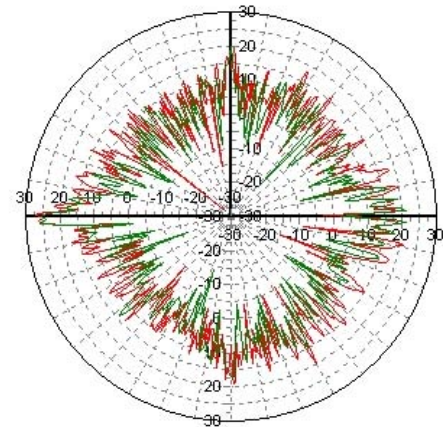(b) Converged IPO currents.

Fig. 16. Surface current distributions over SLICY for 225° azimuth, 10° elevation and vertical polarization at 9 GHz.

Fig. 17. CAD model for ZSU-23-4.

(a) Vertical polarization.

(b) Horizontal polarization.

Fig. 18. IPO results for co-polarized mono-static RCS of ZSU-23-4 compared to the results obtained by using MSPO for 0°-360° azimuth and 30° elevation at 2 GHz.
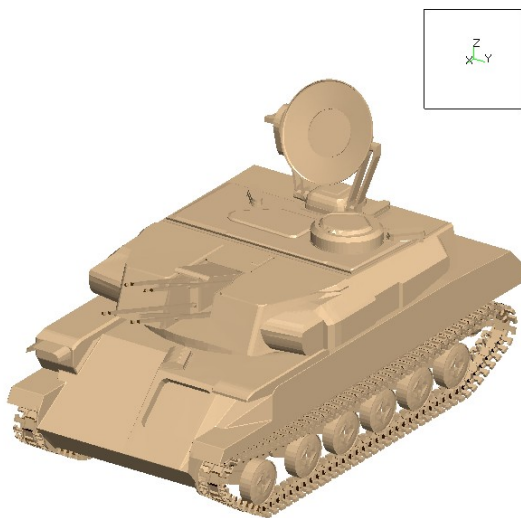
Generic Tank Model

A generic tank shown in Figure 21 was considered last. The mono-static RCS of this target, which is 609.60 x 325.12 x 218.44 cm in size, was computed by using IPO at 10 GHz for co-polarized fields. CAD model for the target consists of 521,932 triangular facets at this frequency, corresponding to about 10 facets per square wavelength. IPO results are shown in comparison with the results obtained by using XPatch and measured data in Fig. 22 for 0-360° azimuth and 10° elevation. Overall, the IPO results
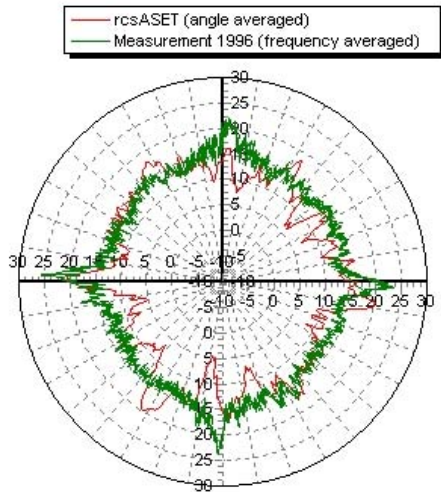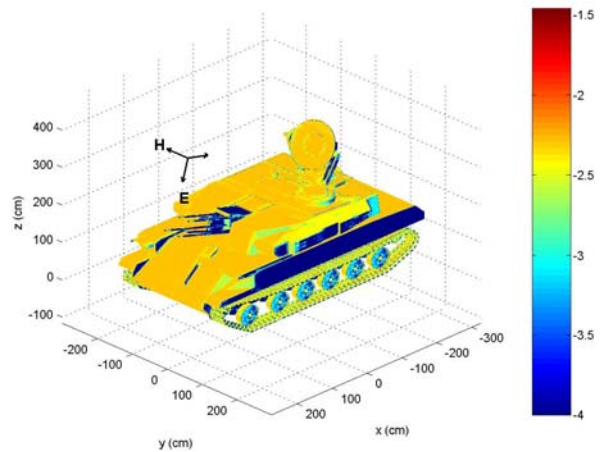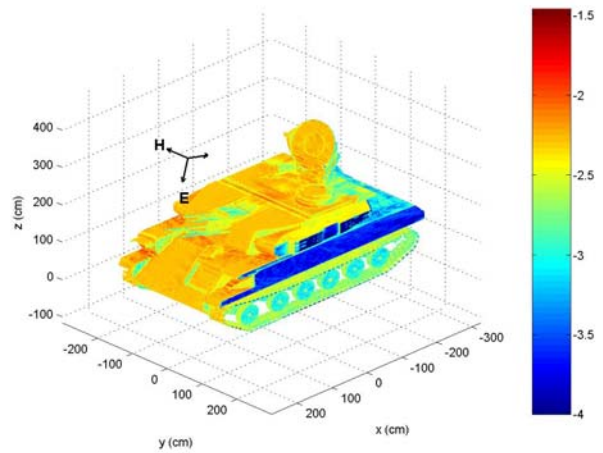
(a) Vertical polarization.
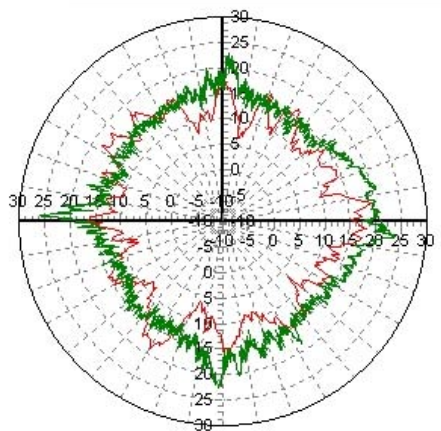
(b) Horizontal polarization.

Fig. 19. IPO results for co-polarized mono-static RCS of ZSU-23-4 compared to measured data for 0-360° azimuth and 30° elevation at 9 GHz. The IPO results are angle averaged whereas the measured data is frequency averaged over a 2 GHz bandwidth, and the measurements were performed with the target on an absorber-covered in-ground metal turntable whereas the IPO results are in free space.

are closer to the measured data than the results generated by using Xpatch. It should be noted that the IPO results are angle averaged whereas the others are frequency averaged over a 0.66 GHz bandwidth [25]. First-order PO and converged IPO current distributions at 10 GHz for 0° azimuth and 30° elevation are also shown in Fig. 23.

(a) First-order PO currents.

(b) Converged IPO currents.

Fig. 20. Surface current distributions over ZSU-23-4 for 0° azimuth, 15° elevation and vertical polarization at 9 GHz.
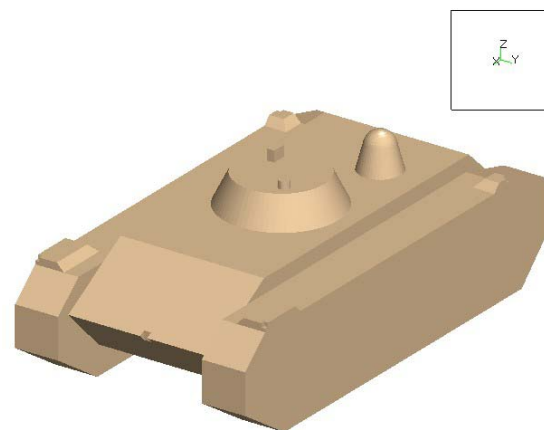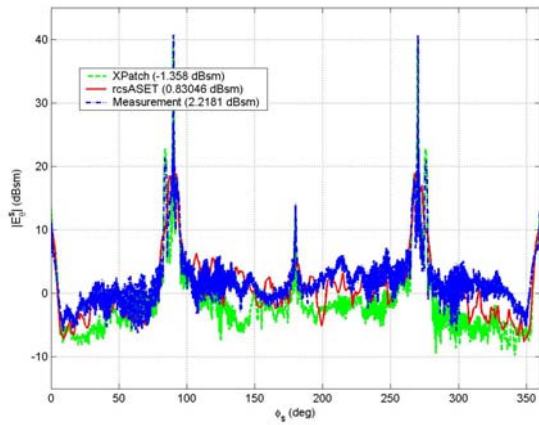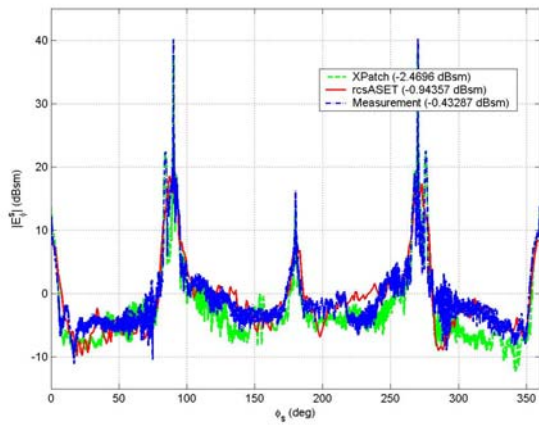

Fig. 21. CAD model for the generic tank.

corner trihedral, SLICY, ZSU-23-4 and generic tank were computed at high frequencies by using

(a) Vertical polarization.
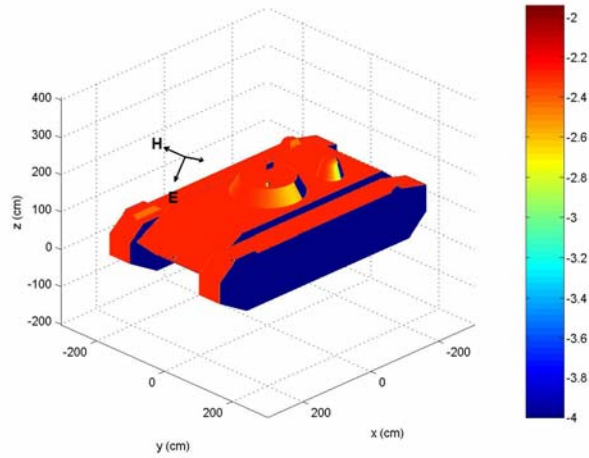

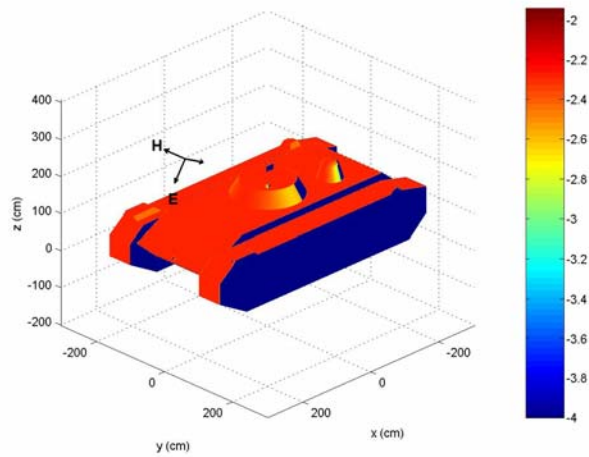(a) First-order PO currents.

(b) Horizontal polarization.

Fig. 22. IPO results for co-polarized mono-static RCS of the generic tank compared to the results obtained by using XPatch and measured data for 0-360° azimuth and 10° elevation at 10 GHz. Xpatch and measured data are frequency averaged over a 0.66 GHz bandwidth.

(b) Converged IPO currents.

Fig. 23. Surface current distributions over the generic tank for 0° azimuth, 30° elevation and vertical polarization at 10 GHz.

Parallelization of the rcsASET code helped reduce the computation time significantly. The mono-static RCS is computed for vertical and horizontal polarizations at each scattering angle in the code. Because of the low memory requirement of IPO, parallelization of the code makes it possible to allocate the RCS computation for each polarization and small ranges of scattering angles to a different processor. The efficiency of the code is greatly improved by computing the IPO currents for multiple angular excitations simultaneously (typically 10 to 20) so that the terms in (10) do not have be recomputed for every angle. The mono-static RCS patterns of the tilted trihedral, smooth

the parallel version of the rcsASET code to demonstrate the reduction in computation time. Results were obtained in a few days with the parallel version of the code on multiple processors, which would otherwise take a few years to get the same results with its serial version on a single processor. The computation time with the parallel version of the code are shown in Table 1 for the benchmark targets considered.

Table 1: Savings in computation time with the parallel version of the rcsASET code.

Target	Freq. (GHz)	Number of facets	Number of angles	Number of processors	Max. time per proc. (hours)
Tilted trihedral	94	1,092,548	362	91	84
Smooth corner trihedral	94	764,224	362	91	69
SLICY	34	3,960,290	360	180	116
ZSU-23-4	9	1,027,796	720	360	91
Generic tank	10	2,267,544	360	360	70

The rcsASET code for RCS pattern computations has been further improved by using it in conjunction with MBPE for fast angle or frequency sweeps. When MBPE is employed adaptively, the reduction in computation time changes with M and N. Different targets may also have different optimum values for M and N. Variations in computation time with the values of M and N are shown in Fig. 24 for frequency and azimuth sweeps in computing the RCS of the tilted trihedral and smooth corner trihedral, respectively. Approximately 19 and 14 times speed-up can be achieved respectively in the frequency and azimuth sweeps shown in Fig. 24 with optimum values of M and N.

Accuracy is not much compromised with MBPE, even though substantial speed-up is achieved with MBPE as was shown in Fig. 24. RCS results with and without MBPE, and MBPE points are shown in Figs. 25, 26 and 27 respectively for the tilted trihedral, smooth corner trihedral and SLICY where MBPE points are not always uniformly distributed due to adaptive implementation of MBPE. It is shown in Figs. 25-27 that MBPE can accurately capture the nulls in the RCS even when there are no MBPE points at these nulls. Thus, MBPE is much more than a regular interpolation method. Although optimum values of M and N giving the lowest computation time are not investigated for SLICY, the values of M and N that are used in MBPE yield 9 times speed-up for 1 MHz frequency increment as shown in Fig. 27.

V. CONCLUSIONS

The IPO method has been shown to be very efficient, robust and accurate for handling RCS problems involving electrically large and realistically complex structures. It is physically insightful for capturing multiple interactions up to
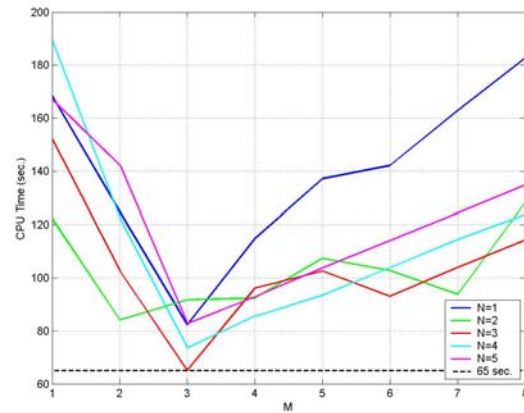
(a) Frequency sweep for tilted trihedral with 45° azimuth and 10° elevation at 2-3 GHz where the lowest time is obtained with M=3 and N=3 resulting in 19 times speed-up for 1 MHz frequency increment. Time for full sweep is 1,235 seconds.
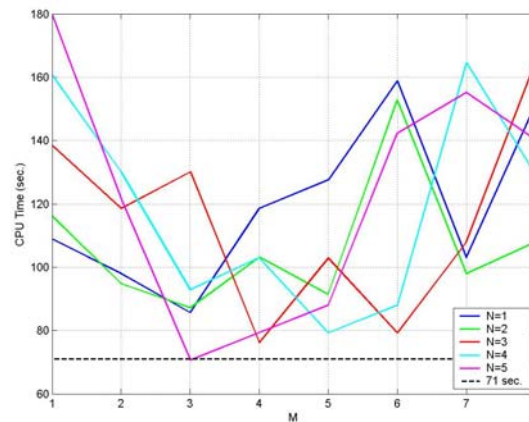
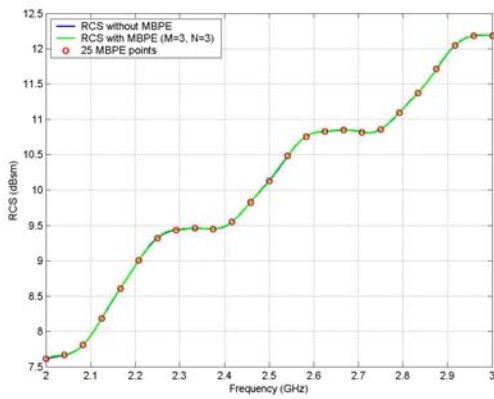(b) Azimuth sweep for smooth corner trihedral with 0-90° azimuth and 10° elevation at 3 GHz where the lowest time is obtained with M=3 and N=5 resulting in 14 times speed-up for 0.1° azimuth increment. Time for full sweep is 994 seconds.

Fig. 24. Variation of mono-static RCS computation time with values of M and N.

a specified order via the number of iterations. It tends to be more efficient but less accurate than rigorous numerical methods, and more accurate but less efficient than ray tracing methods. As such, it bridges the gap between these two extremes with a viable solution for practical engineering problems. Typically, an order of magnitude reduction in the number of unknowns with respect to purely numerical methods is possible, while the memory requirement is O(*N*). Another order of magnitude reduction is possible by combining the MPBE method with IPO for generating swept frequency and angle patterns. The IPO solution has also been applied to the performance analysis of antennas installed on realistic platforms such as aircraft and ships [26].

(a) Vertical polarization.

(a) Vertical polarization.

(b) Horizontal polarization.

(b) Horizontal polarization.

Fig. 26. IPO azimuth sweep results for co-polarized mono-static RCS of smooth corner trihedral with (M=3 and N=5 as optimum values) and without MBPE, and 33 MBPE points for 0-90° azimuth and 10° elevation at 3 GHz.
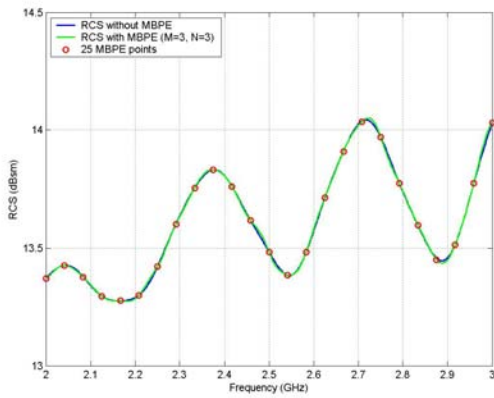
Fig. 25. IPO frequency sweep results for co-polarized mono-static RCS of tilted trihedral with (M=3 and N=3 as optimum values) and without MBPE, and 25 MBPE points for 45° azimuth and 10° elevation at 2-3 GHz.
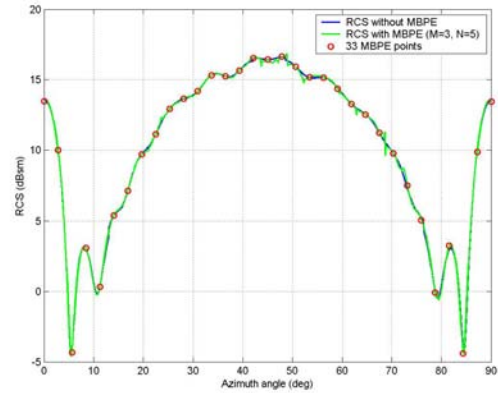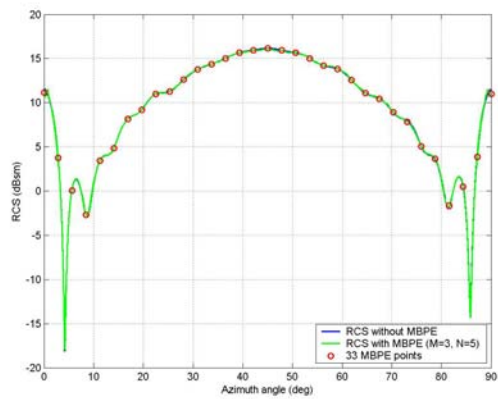

(a) Vertical polarization.
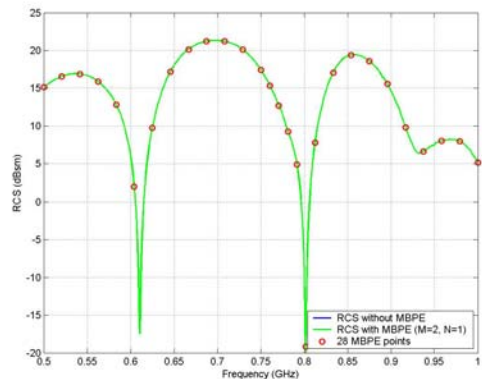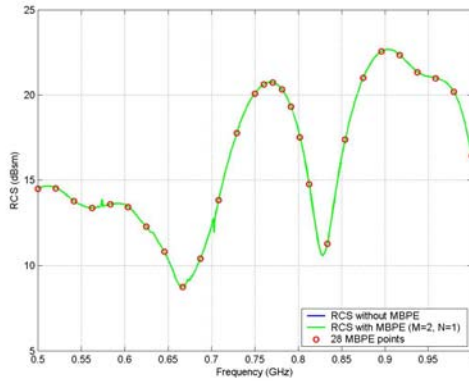
(b) Horizontal polarization.

Fig. 27. IPO frequency sweep results for co-polarized mono-static RCS of SLICY with (*M*=2, *N*=1) and without MBPE, and 28 MBPE points for 0° azimuth and 30° elevation at 0.5-1 GHz. Although the *M* and *N* values used may not be optimum, 9 times speed-up is achieved for 1 MHz frequency increment.

REFERENCES

[1]   F. Obelleiro, J. L. Rodriguez and R. J. Burkholder, "An iterative physical optics approach for analyzing the electromagnetic scattering by large open-ended cavities," *IEEE Trans. Antennas Propagat.*, vol. 43, No. 4, pp. 356-361, April 1995.

[2]   R. J. Burkholder, "A fast and rapidly convergent iterative physical optics algorithm for computing the RCS of open-ended cavities," *App. Comput. Electro. Soc. J.,* vol. 16, No. 1, pp. 53-60, March 2001.

[3]   R. J. Burkholder and T. Lundin, "Forward-backward iterative physical optics algorithm for computing the RCS of open-ended cavities," *IEEE Trans. Antennas Propagat.,* vol. 53, No. 2, pp. 793-799, Feb. 2005.

[4]   R. F. Harrington, *Field computation by moment methods.* New York: Macmillan, 1968.

[5]   J. M. Jin, *The Finite Element Method in Electromagnetics*, New York: Wiley, 2002.

[6]   S. Velamparambil, W. C. Chew and J. M. Song, "10 Million Unknowns: Is it that Big?" *IEEE Antennas Propagat. Mag.*, vol. 45, No. 2, pp. 43-58, April 2003.

[7]   B. Stupfel, "A Fast-Domain Decomposition Method for the Solution of Electromagnetic Scattering by Large Objects," *IEEE Trans.*

[8]   Y. J. Li and J. M. Jin, "A Vector Dual-Primal Finite Element Tearing and Interconnecting Method for Solving 3-D Large-Scale Electromagnetic Problems," *IEEE Trans. Antennas Propagat.,* vol. 54, No. 10, pp. 3000-3009, Oct. 2006.

[9]   H. Ling, R. C. Chou and S. W. Lee, "High-Frequency RCS of Open Cavities with Rectangular and Circular Cross Sections," *IEEE Trans. Antennas Propagat.*, vol. 35, No. 4, pp. 391-398, April 1987.

[10] G. Crabtree, "A Numerical Quadrature Technique for Physical Optics Scattering Analysis," *IEEE Trans. Magnetics*, vol. 27, No. 5, pp. 4291-4294, Sep. 1991.

[11] P. H. Pathak and R. J. Burkholder, "High frequency scattering," *Section 1.5.2 in Scattering: Scattering and Inverse Scattering in Pure and Applied Science*, pp. 245-276, Edited by E.R. Pike and P. Sabatier, Academic Press, Ltd., London, 2002.

[12] F. S. de Adana, S. Nieves, E. Garcia, I. Gonzalez, O. Gutierrez and M. F. Catedra, "Calculation of the RCS from the Double Reflection Between Planar Facets and Curved Surfaces," *IEEE Trans. Antennas Propagat.*, vol. 51, No. 9, pp. 2509-2512, Sep. 2003.

[13] J. Baldauf, S. W. Lee, L. Lin, S. K. Jeng, S. M. Scarborough and C. L. Yu, "High-Frequency Scattering from Trihedral Corner Reflectors and Other Benchmark Targets – SBR Versus Experiment," *IEEE Trans. Antennas Propagat.*, vol. 39, No. 9, pp. 1345-1351, Sep. 1991.

[14]   XPATCH: A High-Frequency Electromagnetic-Scattering Prediction Code and Environment for Complex Three-Dimensional Objects," *IEEE Antennas Propagat. Mag.*, vol. 36, No. 1, pp. 65-69, Feb. 1994.

[15] P. H. Pathak, "Techniques for High Frequency Problems," in *Antenna Handbook, Theory, Application and Design*, edited by Y. T. Lo and S. W. Lee, Van Nostrand Reinhold Co. Inc., New York, 1988.

[16] S. H. Park, K. K. Park, J. H. Jung, H. T. Kim and K. T. Kim, "Construction of Training

Database Based on High Frequency RCS Prediction Methods for ATR," *J. of Electromagnetic Waves App.,* vol. 22, No. 5-6, pp. 693-703, 2008.

[17] F. Obelleiro, M. G. Araujo and J. L. Rodriguez, "Iterative Physical Optics Formulation for Analyzing Large Waveguildes with Lossy Walls," *Microwave Opt. Tech. Lett.*, vol. 28, No. 1, pp. 21-26, Jan. 5, 2001.

[18] G. H. Golub and C. F. Van Loan, *Matrix Computations*, Third Edition, The Johns Hopkins University Press, Baltimore, 1996.

[19] C. C. Lu and W. C. Chew, "Fast Far-Field Approximation for Calculating the RCS of Large Objects," *Microwave Opt. Tech. Lett.,* vol. 8, No. 5, pp. 238-241, 1995.

[20] R. Coifman, V. Rokhlin and S. Wandzura, "The Fast Multipole Method for the Wave Equation: A Pedestrian Prescription," *IEEE Antennas Propagat. Mag.,* vol. 35, No. 3, pp. 7-12, 1993.

[21] Y. E. Erdemli, J. Gong, C. J. Reddy and J. L. Volakis, "Fast RCS Pattern Fill Using AWE Technique," *IEEE Trans. Antennas Propagat.,* vol. 46, No. 11, pp. 1752-1753, Nov. 1998.

[22] W. O. Coburn, C. D. Le, C. S. Kenyon, W. A. Spurgeon, and S. L. Carter, "The RCS of a Canonical Corner Target Including Lossy Dielectric Materials," *Army Research Lab Report* ARL-TR-3112, LIMITED, 2003.

[23] W. A. Spurgeon, C. D. Le, W. O. Coburn, R. L. Bender, and S. R. Stratton, "Modeling and Measuring the Radar Cross Section of Two Trihedrons at X, Ka, and W Bands*," Army Research Lab Report* ARL-TR-3098, LIMITED, 2003.

[24] W. O. Coburn and C. D. Le, "An Investigation of the ZSU-23-4 Radar Cross Section at X-Band," *Army Research Lab Report* ARL-TR-3003, 2003.

[25] W. Spurgeon, W. Nixen, J. Sizemore and S. Carter, "Modeling and Validation of the Effects of a Ground Plane on the RCS of a Second Revised T5M3 Ground Vehicle Simulator," *Army Research Lab Report* ARL-TR-3391, January 2005.

[26] R. J. Burkholder, P. H. Pathak, K. Sertel, R. J. Marhefka, J. L. Volakis and R. W. Kindt, "A Hybrid Framework for Antenna/Platform Analysis," Invited paper, *Applied Computational Electromagnetics Society Journal, Special issue on array antennas*, vol. 21, No. 3, pp. 177-195, Nov. 2006.

Robert J. Burkholder received the B.S., M.S., and Ph.D. degrees in electrical engineering from The Ohio State University, Columbus, in 1984, 1985, and 1989, respectively. Since 1989, he has been with The Ohio State University ElectroScience Laboratory, Department of Electrical and Computer Engineering, where he is currently a Senior Research Scientist and Adjunct Professor. Dr. Burkholder's research specialties are high-frequency asymptotic techniques and their hybrid combination with numerical techniques for solving large-scale electromagnetic radiation, propagation, and scattering problems.

Çağatay Tokgöz received the B.S. degree from Bilkent University, Ankara, Turkey, in 1994, the M.S. degree from the Middle East Technical University, Ankara, Turkey, in 1997, both in electrical and electronics engineering, and the Ph.D. degree in electrical engineering from The Ohio State University, Columbus, OH, in 2002. He has been working for Applied EM, Incorporated, Hampton, VA, as a Senior Research Engineer since 2002. His research interests include closed-form Green's function techniques for stratified media, and asymptotic high-frequency techniques particularly Iterative Physical Optics (IPO) and Uniform Geometrical Theory of Diffraction (UTD) for solving antenna radiation, antenna coupling and radar signature prediction problems associated with electrically large complex structures.

C. J. Reddy received B.Tech. degree in Electronics and Communications Engineering from Regional Engineering College (now National Institute of Technology), Warangal, India in 1983. He received his M.Tech. degree in Microwave and Optical Communication Engineering and Ph.D. degree in Electrical Engineering, both from Indian Institute of Technology, Kharagpur, India, in 1986 and 1988 respectively. Currently, Dr. Reddy is the President and Chief Technical Officer of Applied EM Inc, a small company specializing in computational electromagnetics, antenna design and development. Dr. Reddy also serves as the President of EM Software & Systems (USA) Inc. At EMSS (USA), he is leading the marketing and support of commercial 3D electromagnetic software, FEKO in the US, Canada, Mexico and Central America. Dr. Reddy is a member of the Board of Directors of the Applied Computational Electromagetics Society.

William O. Coburn received his BS in Physics from Virginia Polytechnic Institute in 1984. He received an MSEE in Electro physics in 1991 and Doctor of Science in Electromagnetic Engineering from George Washington University (GWU) in 2005. His dissertation research was in traveling wave antenna design. He has 27 years experience as an electronics engineer at the Army Research Laboratory (formerly the Harry Diamond Laboratories) primarily in the area of CEM for EMP coupling/hardening, HPM and target signatures. He currently is in the RF Electronics Division of the Sensors and Electron Devices Directorate applying CEM tools for antenna design and analysis.